

# Propagation Properties of Pearcey-Gaussian Beam and Interaction of Symmetric Pearcey-Gaussian Beams in Photorefractive Media

Siyuan Pan, Guoxing Huang\*

**Abstract**—The study of the propagation properties of Pearcey-Gaussian beams in photorefractive media is essential for understanding the dynamics of special beams. However, the specific effects of different parameters, such as the truncation factor, chirp factor, refractive coefficient, and beam spacing, on the propagation properties of a single Pearcey-Gaussian beam and the interactions between two Pearcey-Gaussian beams need to be clarified. This paper analyzes the dynamical properties of Pearcey-Gaussian beams and their interactions using a stepwise Fourier method. The results show that the truncation factor regulates the intensity distribution of the optical field, the initial chirp factor controls the deflection direction, and the refractive coefficient modulates the spatial soliton respiration period of a single beam. In a double-beam setup, the refractive coefficient and beam spacing affect the repulsive force, while the chirp factor alters the number of solitons. This study provides a theoretical basis for understanding the exceptional beam propagation dynamics.

**Index Terms**—Pearcey-Gaussian; Propagation; Interaction; Photorefractive Media

## I. INTRODUCTION

In 1946, T. Pearcey [1] analyzed the structure of cylindrical electromagnetic waves' focal dispersion line field through many mathematical calculations and described this field with an integral expression, i.e., the Pearcey function. With the continuous development of science and technology, in 2012, Ring [2] and others applied the Pearcey function to research in optics and further explored the propagation theory of the Pearcey beam. The study showed that Pearcey beams exhibit unique propagation properties, such as form invariance, self-focusing, and self-healing. Inspired by these unique optical properties, many studies have been reported. Since 2018, many scholars have made circular Pearcey beams [3], ring Pearcey beams [4], vortex Pearcey beams [5], elliptical Pearcey beams [6], and odd Pearcey beams [7] by continuously improving the design of Pearcey beams. In

experiments, Pearcey-Gaussian beams can be generated by modulating Pearcey beams with Gaussian beams to obtain Pearcey beams with finite energy without losing their properties [8, 9, 10]. In 2021, analytical solutions describing the dynamic behavior of Pearcey-Gaussian beams propagating in free space were provided by Zang [11] et al. Their study focused on the double-focusing behavior of one-dimensional quadratically chirped Pearcey-Gaussian beams, highlighting the complex nature of the propagation of these beams. In 2023, Wen [12] et al. explored the generation of periodic evolutionary modes of Pearcey-Gaussian beams with side flaps in the presence of parabolic potential interactions, revealing their complex evolutionary patterns. These studies help to deeply explore the dynamic properties of Pearcey beams and open up new possibilities for applications in optics. In recent years, researchers have conducted in-depth studies on the propagation properties of Pearcey beams in different fiber media, which include linear media [13], Kerr media [14], parabolic media [15], strongly nonlocal media [16], multimode fibers [17], and Gaussian potential media [18]. However, studies have yet to be reported on the propagation properties of Pearcey-Gaussian beams in photorefractive media.

A photorefractive medium is a medium that is capable of producing light-sensitive refractive coefficient changes by light-induced periodic changes within the crystal [19]. This material provides a good platform for studying the propagation of light beams in nonlinear media [20]. Photorefractive media have unique effects [21, 22, 23], as the photorefractive effect causes the refractive index to change when light shines on the medium, allowing control over light propagation through phenomena like self-acceleration, self-focusing, and self-defocusing. And Pearcey beams, as a new type of special beams, have a wide range of prospects for practical applications. Therefore, it is of great theoretical value to investigate the propagation of Pearcey-Gaussian beams in photorefractive media.

Previously, researchers have discussed the propagate properties of different beams in photorefractive media, such as Airy beams [24] and initial elliptically polarized Gaussian beams [25]. However, studies on the evolutionary properties of oscillating solitons of Pearcey-Gaussian beams in photorefractive media have yet to be reported. To better understand the evolution of the peak power and residual part of the detached soliton generated by the Pearcey-Gaussian beam in the photorefractive medium, as well as to manipulate

Manuscript received August 9, 2024; revised April 1, 2025.

This work was supported by the National Natural Science Foundation of China (No. 62101495).

Siyuan Pan is a graduate student of the College of Information Engineering, Zhejiang University of Technology, Hangzhou 310023, China (e-mail: psy1791407136@163.com).

Guoxing Huang is an associate professor of the College of Information Engineering, Zhejiang University of Technology, Hangzhou 310023, China (corresponding author to provide phone: +86-13136196373; e-mail: hgx05745@zjut.edu.cn).

the detached soliton more efficiently, this paper analyzes in detail the effects of the refractive coefficient of the photorefractive medium, the chirp factor and the truncation factor of the Pearcey-Gaussian beams, as well as the impact of the double-beam spacing of the trailing-in-front versus the trailing-in-front on the evolutionary characteristics of the detached soliton. The results of this paper provide some theoretical basis for applying photorefractive media in all-optical control.

## II. THEORETICAL MODEL AND CALCULATION METHOD

Considering the one-dimensional case, the normalized Nonlinear Schrödinger Equation (NLSE) for the propagation of a beam along the  $z$ -axis in a photorefractive medium under the paraxial approximation can be described as [23]:

$$i \frac{\partial q}{\partial \xi} + \frac{1}{2} \frac{\partial^2 q}{\partial \eta^2} - \beta \frac{q}{1+|q|^2} = 0 \quad (1)$$

Where  $q(\eta, \xi)$  is the normalized complex amplitude envelope of the light wave,  $\eta = x/x_0$  and  $\xi = z/x_0^2$  are the dimensionless transverse and longitudinal coordinates normalized by the beam width  $x_0$  and the Rayleigh distance  $kx_0^2$ , respectively,  $k = 2\pi n_e/\lambda_0$  is the number of waves in the crystal,  $n_e$  is the refractive coefficient of the crystal when it is unperturbed, and  $\lambda_0$  is the wavelength of the light wave in free space;  $-\beta q/(1+|q|^2)$  describes the nonlinear drift of the crystal, with the parameter  $\beta = (k_0 x_0)^2 (n_e^4 r_{\text{eff}}/2) E_0$  is the refractive coefficient;  $r_{\text{eff}}$  is the effective electro-optical coefficient, and  $E_0$  is the applied electric field.

To study the propagation characteristics of a single beam, the wave function expression for the initial input Pearcey-Gaussian beam is given as follows:

$$\varphi(x, 0) = Pe(x, 0) \exp(-\sigma x^2) \exp(icx) \quad (2)$$

Where  $\sigma$  is the truncation factor,  $c$  is the chirp factor, and  $Pe(x, 0)$  is the one-dimensional Pearcey function. The expression of  $Pe(x, 0)$  is as follows:

$$Pe(x, 0) = \int_{-\infty}^{+\infty} ds \exp\left[i(as^4 + s^2 x/b)\right] \quad (3)$$

Where  $a$  is the coefficient of the integral term and  $b$  is the scaling factor.

Fig. 1(a) demonstrates the effect of different truncation factors  $\sigma$  on the intensity distribution of the Pearcey-Gaussian beam. The beam's intensity distribution exhibits an asymmetric trailing oscillation feature, in which the central peak has the highest energy intensity and multiple attenuated side flaps on the left side, forming a long trailing tail. As  $\sigma$  increases, the beam gradually converges to a Gaussian-type distribution from the multi-peak structure, and the energy of the side flaps gradually decreases. This indicates that the truncation factor  $\sigma$  can regulate the relative intensity and distribution characteristics of the central peak and the side flaps. Fig. 1(b) shows the Pearcey-Gaussian beam's peak intensity and peak position as a function of the logarithm of the truncation factor  $\sigma$ . The black curve in the figure indicates the peak intensity, and the red curve indicates the peak position. As the logarithmic value of  $\sigma$  increases from -4 to -2.5, the peak intensity slowly and gradually decreases from 6.9 to 6.7. As the logarithmic value of  $\sigma$  increases from -2.5 to -1.2, the peak intensity accelerates and decreases from 6.7 to 4.5. At the same time, as the logarithmic value of  $\sigma$

increases from -4 to -2.5, the peak position slowly increases from -2.2 to -2.1. As the logarithmic value of  $\sigma$  -2.5 increases to -1.2, the peak position accelerates from -2.1 to -1.4. The results show that when the logarithm of  $\sigma$  is small, the effects on the peak power and peak position are minor, while when the logarithm of  $\sigma$  is large, the effects are significant. Fig. 1(c) demonstrates the impact of different chirp coefficients  $c$  on the phase distribution of the Pearcey-Gaussian beam. The phase of each flap varies continuously from  $-\pi$  to  $\pi$ . The positive or negative chirp coefficient determines whether the phase change is overtaken or lagged. Positive chirp (blue and cyan lines) leads to phase overshooting, while negative chirp (red line) leads to phase lag. This phase variation reflects the modulation of the phase front within the beam and affects the propagation characteristics of the beam, such as focusing ability and self-similarity. The properties of phase modulation are essential for shaping and controlling the beam in optical communication systems and can be used to regulate the beam's propagation characteristics and improve the system's propagation performance.

A more complex incident beam should be constructed to study the interaction of Pearcey-Gaussian beams. The beam is composed of Pearcey-Gaussian beams with leading and trailing tails, emitted in parallel [Fig. 2 (a)].  $Pe_+(x, 0)$  is the one-dimensional tails leading Pearcey function. The expression is as follows:

$$Pe_+(x, 0) = \int_{-\infty}^{+\infty} ds \exp\left[i(as^4 + s^2 x/b)\right] \quad (4)$$

$Pe_-(x, 0)$  is the one-dimensional tails trailing Pearcey function [Fig. 2 (b)]. The expression is as follows:

$$Pe_-(x, 0) = \int_{-\infty}^{+\infty} ds \exp\left[i(as^4 - s^2 x/b)\right] \quad (5)$$

The expression for two Pearcey-Gaussian beams incident in parallel is as follows:

$$q(\eta, \xi = 0) = \left\{ \begin{array}{l} A_1 \times Pe_+[(\eta - B)] \exp[a(\eta - B)] + \\ A_2 \times Pe_-[-(\eta + B)] \exp[-a(\eta + B)] \exp(i\varphi) \end{array} \right\} \quad (6)$$

Where  $A_1$  and  $A_2$  are the amplitudes of the two Pearcey-Gaussian beams with trailing tails in front and behind, respectively,  $A_1 = A_2 = 1$ ;  $B$  is the spacing parameter of the two Pearcey-Gaussian beams;  $\varphi$  is the relative phase of the two beams,  $\varphi = 0$  indicates that the two Airy beams are in-phase, and  $\varphi = \pi$  indicates that the two Airy beams are out-of-phase. To better reflect the propagation characteristics of the Pearcey-Gaussian beams, the variations of the center of gravity  $x_c$  and the intensity  $I$  are chosen for the description.

$$x_c = \frac{\int_{-\infty}^{\infty} x |q|^2 dx}{\int_{-\infty}^{\infty} |q|^2 dx} \quad (7)$$

$$I = \int_{-\infty}^{\infty} |q|^2 dx \quad (8)$$

The Split-Step Fourier Method (SSFM) is a widely used numerical method for solving the NLSE, especially in the field of fiber-optic communication for simulating the propagation of optical pulses. According to SSFM, the above equation is decomposed into a linear part and a nonlinear part:

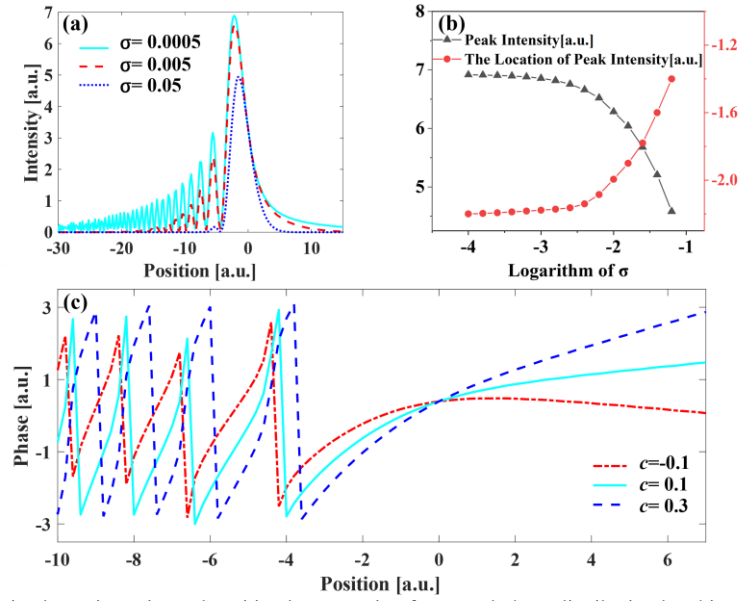


Fig. 1 Modulation of Pearcey-Gaussian beam intensity and position by truncation factor and phase distribution by chirp. When  $\beta = 4$ ,  $c = 0$ ,  $a = b = 1$ , (a) intensity profiles of Pearcey-Gaussian beams with three different truncation factors  $\sigma$ ; (b) plot of the relative energy of the main peaks of the Pearcey-Gaussian beams vs. their positions as a function of the logarithmic variation of the truncation factors; and (c) plot of the phase distributions of the Pearcey-Gaussian beams with different chirp factors  $c$  when  $\sigma = 0.0005$ .

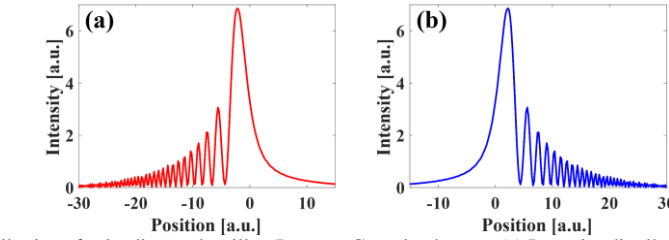


Fig. 2 Comparison of intensity distributions for leading and trailing Pearcey-Gaussian beams. (a) Intensity distribution of the Pearcey-Gaussian beam when  $\beta = 4$ ,  $c = 0$ ,  $\sigma = 0.001$ ,  $b = 1$ ; (b) Intensity distribution of the Pearcey-Gaussian beam when  $\beta = 4$ ,  $c = 0$ ,  $\sigma = 0.001$ ,  $b = -1$ .

$$i \frac{\partial q}{\partial \xi} + \frac{1}{2} \frac{\partial^2 q}{\partial \eta^2} = 0 \quad (9)$$

$$i \frac{\partial q}{\partial \xi} - \frac{\beta q}{1 + |q|^2} = 0 \quad (10)$$

At the initial position  $\xi = 0$ , the input light field  $q(0, \eta)$  is Fourier transformed into the frequency domain:

$$\hat{q}(0, \omega) = \mathcal{F}\{q(0, \eta)\} \quad (11)$$

Where  $\mathcal{F}$  denotes the Fourier transform operation and  $\omega$  is the frequency variable. Next, in the frequency domain, the linear part is half-stepped and the half-step propagation of the linear part is computed, by multiplying it by the corresponding phase shift factor:

$$\hat{q}(\xi + \Delta\xi/2, \omega) = \hat{q}(\xi, \omega) \exp\left(-i \frac{\omega^2 \Delta\xi}{4}\right) \quad (12)$$

In this equation  $\Delta\xi$  is the step size along the direction of  $\xi$ .

The inverse Fourier transform of the frequency-domain light field  $\hat{q}(\xi + \Delta\xi/2, \eta)$ , which has undergone a half-step linear process, is returned to the time domain:

$$q(\xi + \Delta\xi/2, \eta) = \mathcal{F}^{-1}\{\hat{q}(\xi + \Delta\xi/2, \omega)\} \quad (13)$$

Where  $\mathcal{F}^{-1}$  denotes the inverse Fourier transform operation. In the time domain, the nonlinear part is processed, and the light field is adjusted in phase accordingly by directly calculating the influence of nonlinear effects:

$$q(\xi + \Delta\xi, \eta) =$$

$$q(\xi + \Delta\xi/2, \eta) \exp\left(-i \frac{\beta \Delta\xi}{1 + |q(\xi + \Delta\xi/2, \eta)|^2}\right) \quad (14)$$

The time-domain light field  $q(\xi + \Delta\xi, \eta)$ , which has been nonlinearly processed, is again Fourier transformed into the frequency domain to obtain:

$$\hat{q}(\xi + \Delta\xi, \omega) = \mathcal{F}\{q(\xi + \Delta\xi, \eta)\} \quad (15)$$

In the frequency domain, the linear part is again half-stepped to complete the calculation of the complete one-step  $\Delta\xi$ :

$$\hat{q}(\xi + \Delta\xi, \omega) = \hat{q}(\xi + \Delta\xi, \omega) \exp\left(-i \frac{\omega^2 \Delta\xi}{4}\right) \quad (16)$$

The above steps are repeated for each step  $\Delta\xi$ , iteratively computed from  $\xi = 0$  to the final position until the entire propagation process is complete.

### III. ANALYSIS OF RESULTS

#### A. Propagation properties of Pearcey-Gaussian beam in photorefractive media

It has been found that photorefractive spatial solitons can be formed when diffraction-induced broadening is balanced with compression caused by the modulation effect of the photorefractive medium. The light beam incident into the photorefractive medium will be localized at a certain position, thus suppressing the diffraction phenomenon to a certain

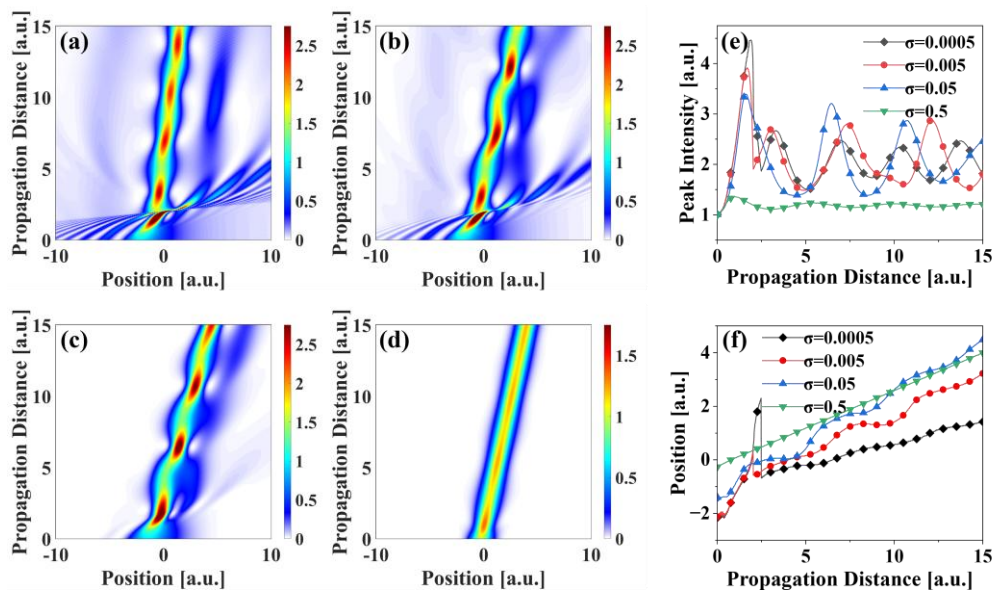


Fig. 3 Spatial evolution of the Pearcey-Gaussian beams with four different truncation factors when  $\beta = 4$ ,  $c = 0$ ,  $a = b = 1$ : (a)  $\sigma = 0.0005$ , (b)  $\sigma = 0.005$ , (c)  $\sigma = 0.05$ , and (d)  $\sigma = 0.5$ ; (e) Plot of the evolution of the peak intensity of the Pearcey-Gaussian beams; and (f) Pearcey-Gaussian plot of the evolution of the main peak position of the beam:  $\sigma = 0.0005$  (black line),  $\sigma = 0.005$  (red line),  $\sigma = 0.05$  (blue line) and  $\sigma = 0.5$  (green line).

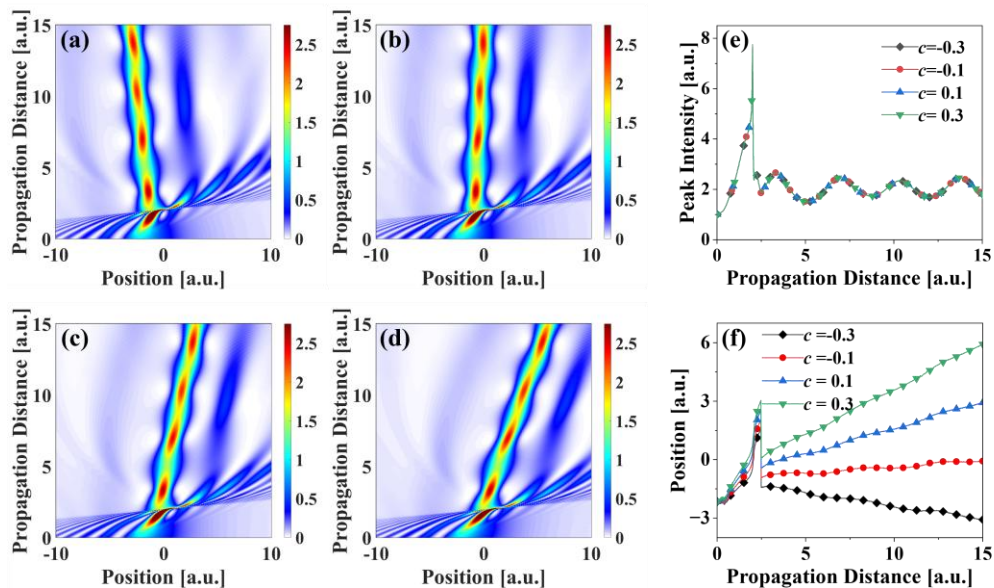


Fig. 4 Spatial evolution of the Pearcey-Gaussian beams with four different chirps when  $\beta = 4$ ,  $\sigma = 0.0005$ , and  $a = b = 1$ : (a)  $c = -0.3$ , (b)  $c = -0.1$ , (c)  $c = 0.1$ , and (d)  $c = 0.3$ ; (e) Plot of the evolution of the peak intensity of the Pearcey-Gaussian beams; and (f) Pearcey-Gaussian evolution of the central peak position of the beam:  $c = -0.3$  (black line),  $c = -0.1$  (red line),  $c = 0.1$  (blue line), and  $c = 0.3$  (green line).

extent and forming a spatial optical soliton. The Pearcey-Gaussian beam undergoes a compression phase at the beginning of the propagation due to the combined effect of diffraction and the nonlinear modulation effect of the photorefractive medium, resulting in an increase in the peak power and an enhancement of the nonlinear modulation effect. The nonlinear effect caused by the photorefractive medium leads to the shedding of a soliton at the main peak of the Pearcey-Gaussian beam, called the shedding refractive breathing soliton. The transverse acceleration of the individual flaps of the beam tends to increase further away from the main flap, leading to the aggregation of the main flap and the side flaps at a propagation distance equal to two. Once this position is crossed, the direction of acceleration becomes negative along the  $x$ -axis, and the beam starts to decelerate in the transverse direction. The more outward the para flap decelerates, the greater the acceleration, leading to

the separation of the main flap and the para flap and the inversion of the intensity distribution, which eventually forms the evolution pattern of focusing flip [Fig. 3(a)]. The truncation factor  $\sigma$  is an important parameter affecting a Pearcey-Gaussian beam's waveform. A numerical simulation study was carried out to investigate the effect of the truncation factor on the generation of breathing solitons in Pearcey-Gaussian beams. Fig. 3 demonstrates the spatial evolution characteristics of the Pearcey-Gaussian beam in the photorefractive medium with different values of the truncation factor  $\sigma$  under the conditions that the refractive coefficient  $\beta = 4$ , the chirp factor  $c = 0$  and the coefficients of the integral term  $a$  and the scaling factor  $b$  are both 1. As seen in Fig. 3(a), the initial state beam shape is an asymmetric trailing structure with the highest energy of the central peak. When the Pearcey-Gaussian beam is propagated in the photorefractive medium, a breathing soliton is shed out of the

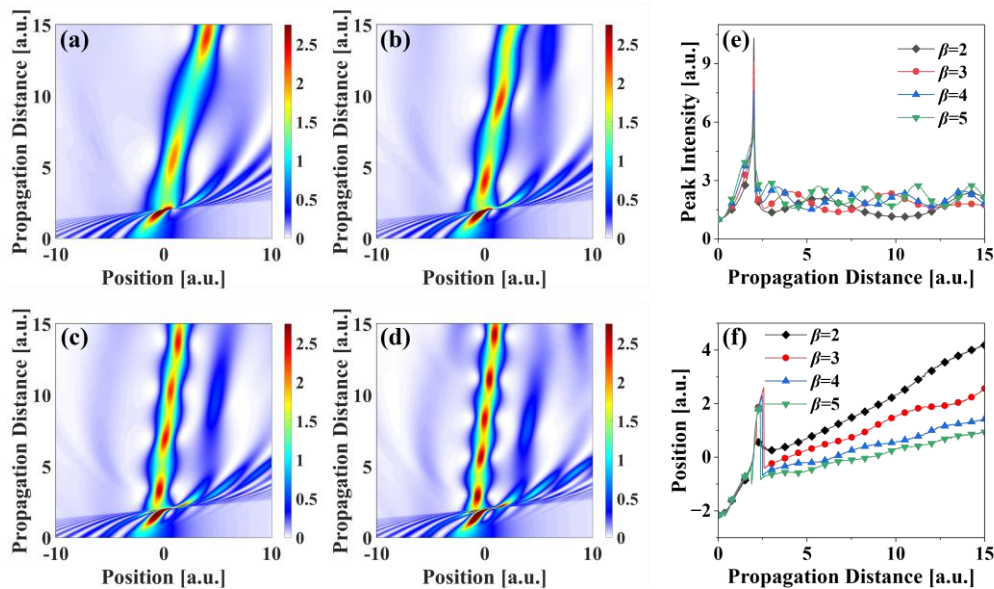


Fig. 5 Spatial evolution of the Pearcey-Gaussian beams with four different refractive index when  $\sigma = 0.0005$ ,  $c = 0$  and  $a = b = 1$ : (a)  $\beta = 2$ , (b)  $\beta = 3$ , (c)  $\beta = 4$  and (d)  $\beta = 5$ ; (e) evolution of the peak intensity of the Pearcey-Gaussian beams; (f) evolution of the central peak position of the Pearcey-Gaussian beam main peak position evolution plots:  $\beta = 2$  (black line),  $\beta = 3$  (red line),  $\beta = 4$  (blue line) and  $\beta = 5$  (green line).

central peak, and at the same time, due to its self-recovery property, a long trailing tail is formed. As  $\sigma$  increases, the beam gradually transitions from a multi-peak structure to a single-peak structure close to a Gaussian distribution. At the same time, the parapet energy in the trailing region significantly decreases and further concentrates in the main peak region, with the total energy remaining constant. Especially when  $\sigma$  is small [Fig. 3(a)-(d)], the paraflap energy distribution is more significant. When  $\sigma$  increases further, the beam gradually shows a linear deflection trend, the paraflap disappears, the main peak energy reaches the maximum value, and the beam loses the lateral self-acceleration property [Fig. 3(c)-(d)]. This indicates that the beam with a smaller truncation factor has a significant trailing effect and multi-peak characteristics. In comparison, the larger truncation factor weakens these characteristics. It concentrates the energy more in the main peak region, resulting in a more concentrated and symmetric intensity distribution of the beam. In addition, the effect of  $\sigma$  on the peak intensity and position is shown in Fig. 3(e)-(f). Specifically, when  $\sigma$  is small, the beam produces significant focusing at a propagation distance of about 2, and deflection occurs after crossing this propagation distance. At this point, the deflection angle decreases following  $\sigma$ . When  $\sigma$  is large, the focusing property of the beam at the propagation distance of 2 is weakened, and a stable deflection state is presented. The above characteristics indicate that  $\sigma$  can significantly regulate the beam's intensity distribution and affect its deflection behavior, providing a feasible strategy for realizing beam modulation.

The chirp factor  $c$  is an important characteristic parameter of Pearcey-Gaussian beams, and numerical simulations were carried out to investigate its effect on the generation of breathing solitons. Figs. 4(a)-4(d) demonstrate the spatial evolution diagrams of Pearcey-Gaussian beams in photorefractive media with different chirp factors  $c$  under the conditions of  $\beta = 4$ ,  $\sigma = 0.0005$ ,  $a = b = 1$ . The results show that the soliton is deflected counterclockwise when  $c < 0$  [Figs. 4(a)-4(b)], and in the clockwise direction when  $c > 0$

[Figs. 4(c)-4(d)], and the angle of the deflection increases with the increase of  $|c|$ . In Fig. 4(e), the beam is focused here at a propagation distance of about 2, and the peak intensity can reach about 8. However, once it crosses 2, the peak intensity decreases sharply and then shows periodic fluctuations. In addition, the figure reveals that  $c$  has no significant effect on the oscillation period and peak intensity of the soliton, indicating that the variation of  $c$  mainly affects the beam deflection rather than the intensity. In Fig. 4(f), the overall dispersion of the beam under different chirp factor parameters demonstrates the difference in the deflection angle of the central peak for different  $c$  values. The beam is collectively deflected with different intensities at a propagation distance of about 2, up to the propagation distance of 3. After crossing this position, the beam recovers and is deflected again. This deflection phenomenon provides the possibility of directional beam modulation in optical communication, i.e., by adjusting the chirp factor, precise control of the beam deflection direction can be achieved, which optimizes the optical device's beam propagation path.

The refractive coefficient  $\beta$  is a critical characteristic parameter of Pearcey-Gaussian beams. Fig. 5 illustrates the evolutionary properties of the Pearcey-Gaussian beam in four different refractive coefficients  $\beta$ . As shown in Fig. 5(a)-(d), the increase of  $\beta$  significantly enhances the peak intensity. Correspondingly, the nonlinear effect in the center region increases, the photorefractive medium has a more remarkable ability to bind the Pearcey-Gaussian beam, and the beam width decreases, which accelerates the breathing frequency of the beam. Fig. 5(e) quantitatively demonstrates the evolutionary trend of the peak intensity, where the beam focuses when the propagation distance is about 2. At the same time, the smaller  $\beta$  is, the higher the peak intensity is. However, when the propagation distance crosses 2, the beam is in a regular breathing state, at which time the smaller  $\beta$  is, the smaller the peak intensity of the beam is. Fig. 5(f) demonstrates the modulation effect of the refractive coefficient on the soliton deflection angle, showing that a larger  $\beta$  decreases the beam deflection angle and thus

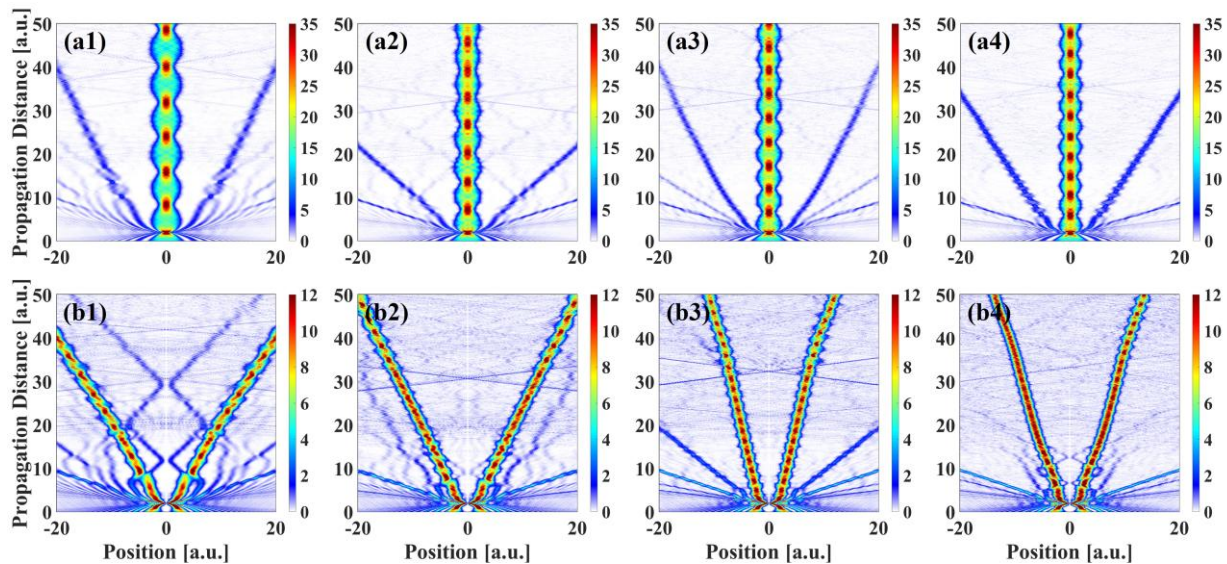


Fig. 6 Interaction of symmetric Pearcey-Gaussian beams in (a1)-(a4) in-phase and (b1)-(b4) anti-phase configurations at different refractive coefficients ( $\sigma = 0.0005$ ,  $c = 0$ ,  $B = 0$ ,  $a = b = 1$ ): (a1)-(b1)  $\beta = 6$ , (a2)-(b2)  $\beta = 8$ , (a3)-(b3)  $\beta = 10$ , and (a4)-(b4)  $\beta = 12$ .

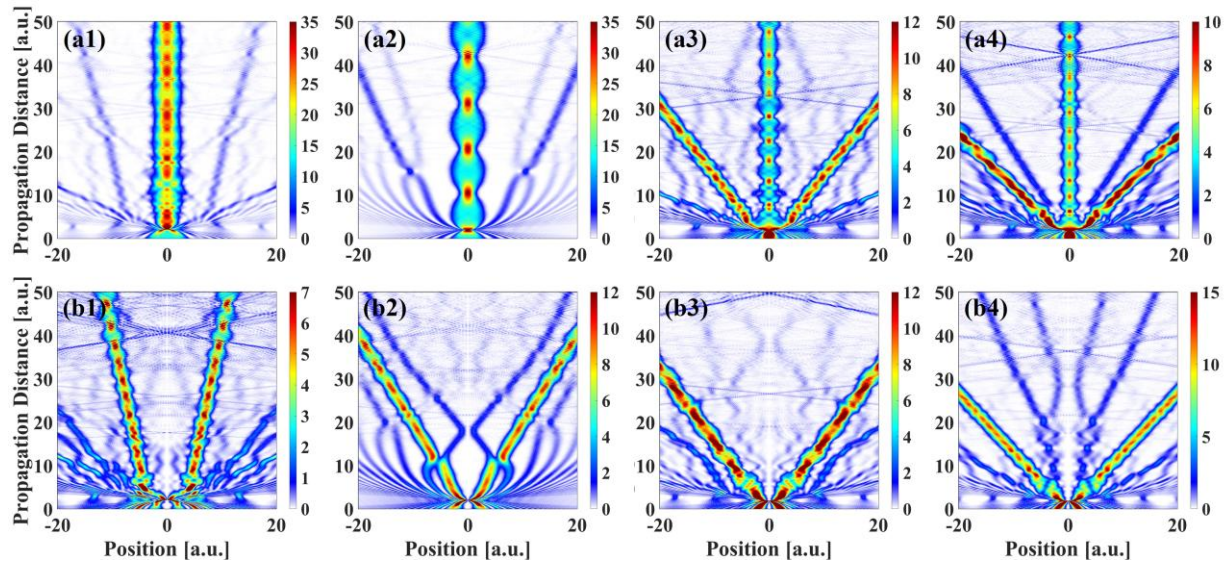


Fig. 7 Interaction of symmetric Pearcey-Gaussian beams in (a1)-(a4) in-phase and (b1)-(b4) anti-phase configurations at different chirps ( $B = 0$ ,  $\sigma = 0.0005$ ,  $\beta = 4$ ,  $a = b = 1$ ): (a1)-(b1)  $c = -0.4$ , (a2)-(b2)  $c = 0$ , (a3)-(b3)  $c = 0.4$ , (a4)-(b4)  $c = 0.5$ .

enhances the focusing characteristics of the beam. This modulation effect of the refractive coefficient provides a feasible strategy for the dynamic control of the soliton behavior in the photorefractive medium, optimizing the periodic evolution of the beam by adjusting  $\beta$  in practical applications.

### B. Interaction of symmetric Pearcey-Gaussian beams in photorefractive media

Fig. 6 demonstrates the in-phase and anti-phase interactions of a symmetric Pearcey-Gaussian beam with the trailing tail in front and the trailing tail in the photorefractive medium for different refractive coefficients  $\beta$ . The two beams are in-phase and anti-phase. In the in-phase propagation, the spacing between the two beams is small. When the interaction of the nonlinear focusing effect and the diffraction effect of the photorefractive medium reaches equilibrium, an attractive force arises between the beams, leading to the aggregation of the beams and shedding of a bundle of breathing solitons, i.e., the main flap forms a single soliton in the bound state [Fig. 6(a1)]. As the  $\beta$  value gradually increases, the period of the breathing soliton shortens, and its

width narrows [Figs. 6(a2)-6(a4)]. In the case of anti-phase propagation, repulsive forces are generated between the beams, forming a pair of breathing solitons linearly deflected in opposite directions at gradually increasing distances [Fig. 6(b1)]. When the value of  $\beta$  gradually increases, the repulsive force is weakened, the deflection angle of the breathing soliton decreases, the distance between the two beams of breathing solitons decreases, the width decreases, and the respiration period is shortened [Fig. 6(b2) - (b4)]. The results show that  $\beta$  has a key role in the two-beam interaction, and its magnitude directly determines the breathing dynamics and width of the soliton and the degree of attraction or repulsion between the beams. In the case of in-phase transmission, the larger the refractive coefficient, the shorter the breathing period, and the narrower the width. In anti-phase transmission, the refractive coefficient can control the change of repulsive force between the breathing soliton pairs; the larger the refractive coefficient, the smaller the deflection angle, and the smaller the repulsive force. Therefore, by adjusting the refractive coefficient, the interaction mode of the beam can be effectively controlled in the photorefractive medium, which provides a theoretical basis for realizing the

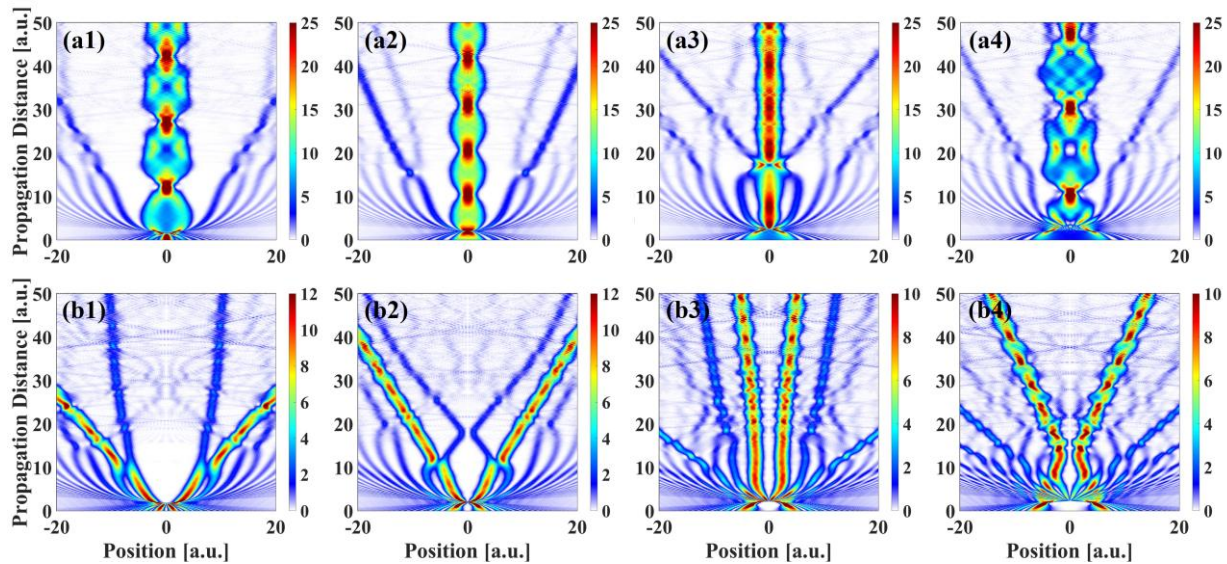


Fig. 8 Interaction of dual Pearcey-Gaussian beams in (a1)-(a4) in-phase and (b1)-(b4) anti-phase configurations at different spacings ( $\sigma = 0.0005$ ,  $c = 0$ ,  $\beta = 4$ ,  $a = b = 1$ ): (a1)-(b1)  $B = -2$ , (a2)-(b2)  $B = 0$ , (a3)-(b3)  $B = 2$ , and (a4)-(b4)  $B = 4$ .

transmission control of multiple beams.

Fig. 7 demonstrates the interaction of two Pearcey-Gaussian beams in the photorefractive medium at different chirp factors  $c$  for both in-phase and anti-phase. When positive and negative Pearcey-Gaussian beams are propagated in the same phase in the photorefractive medium, an attractive force is generated between the beams when  $c = 0$  and the beam spacing is small. When the attractive force is balanced with the photorefractive effect, a beam of breathing solitons is shed [Figs. 7(a1)-7(a2)]. When  $c \neq 0$ , the equilibrium between the attractive force and the photorefractive effect is broken due to the introduction of the chirp factor deflection effect, and the breathing soliton undergoes folding [Figs. 7(a3)-7(a4)]. The results show that the chirp factor  $c$  can control the production of an odd number of breathing solitons for positive and negative Pearcey-Gaussian beams propagated in the same phase. In anti-phase propagation, when  $c = 0$ , a repulsive force is generated between the beams, forming a pair of breathing solitons linearly deflected in opposite directions with gradually increasing distance [Fig. 7(b2)]. When  $c < 0$ , the breathing soliton shed by the positive Pearcey-Gaussian light on the right is deflected in the counterclockwise direction, and the breathing soliton shed by the anti-Pearcey-Gaussian light on the left is deflected in the opposite direction, resulting in a decrease in the distance between the pairs of breathing solitons [Fig. 7(b1)]. When  $c > 0$ , the respiratory soliton shed by the positive Pearcey-Gaussian light on the right is deflected in the clockwise direction, while the respiratory soliton shed by the anti-Pearcey-Gaussian light on the left is again deflected in the opposite direction, leading to an increase in the distance between respiratory soliton pairs [Figs. 7(b3)-7(b4)]. It follows that the chirp factor can control the variation of the repulsive force between the breathing solitons when the double Pierce-Gaussian beam is transmitted in antiphase in the photorefractive medium, i.e., the chirp factor can control the distance between the breathing soliton pairs. When  $c < 0$ , the distance gradually decreases; when  $c > 0$ , the distance gradually increases. The phenomenon indicates that the directional quantitative

regulation of beam solitons can be realized by adjusting the chirp factor. This behavior has potential application to beam transmission in optical communication, i.e., by controlling the chirp factor, the number of beams and interaction modes can be changed, thus realizing the precise control of beams.

Fig. 8 illustrates the interaction of two Pearcey-Gaussian beams in the photorefractive medium at different spacings  $B$  in both in-phase and antiphase. In the in-phase transmission [Fig. 8(a1)-(a4)], when the spacing is small, the beams produce strong attraction and form narrow breathing solitons, and the width of the breathing solitons reaches a minimum at  $B = 2$ . Subsequently, the spacing is further increased, which makes the attraction between the beams gradually weaken, and the width of the breathing soliton gradually increases. That is, centered on  $B = 2$ , the period of the breathing soliton is shortened when the value of  $|B|$  gradually decreases. In anti-phase transmission [Fig. 8(b1)-(b4)], the repulsive force between the beams and the nonlinear effect combine to form a pair of gradually separated breathing solitons linearly deflected in opposite directions [Fig. 8(b2)]. With  $B = 2$  as the center of symmetry, when the value of  $|B|$  is small, the deflection angle is also small; as the spacing increases, the repulsive force is enhanced, and the soliton deflection angle increases. In particular, the beams in Fig. 8(b4) are first attracted upon interaction and then repel each other after elastic collisions, mainly due to the larger spacing. The results show that during in-phase transmission, centered at  $B = 2$ , the larger the value of  $|B|$ , the longer the period and the wider the width of the breathing soliton. In anti-phase transmission, with  $B = 2$  as the center of symmetry, the larger the value of  $|B|$ , the larger the deflection angle of the breathing soliton. This phenomenon suggests that  $B$  not only controls the breathing period and width among the solitons but also affects the deflection behavior of the solitons, providing the possibility of realizing precise control of the beam transmission characteristics by adjusting the beam spacing.

#### IV. CONCLUSION

This study numerically investigates the propagation dynamics of Pearcey-Gaussian beams in photorefractive

media. The results show that the truncation factor of the Pearcey-Gaussian beam can regulate the distribution of its light field intensity during propagation in photorefractive media, and a more significant truncation factor  $\sigma$  significantly reduces the parabolic energy and concentrates it in the central peak region. The chirp factor determines the soliton deflection direction: clockwise for  $c > 0$  and counterclockwise for  $c < 0$ . The refractive coefficient significantly affects space solitons' breathing period and deflection behavior. More significant refractive coefficients enhance the binding effect of the photorefractive medium, which produces higher-frequency breathing cycles and reduces the soliton's deflection angle during the beam's propagation. In the symmetric Pearcey-Gaussian beams with the trailing tail in the front and the trailing tail in the back, the refractive coefficient can effectively control the characteristics of the soliton in both in-phase and anti-phase propagation. In in-phase propagation, the larger the refractive coefficient is, the shorter the breathing period and the narrower the width of the breathing soliton; in anti-phase propagation, the larger the refractive coefficient is, the smaller the repulsive force between the solitons and the smaller the deflection angle. In addition, the chirp factor can change the number of solitons during in-phase propagation, while the number remains constant during anti-phase propagation. The solitons' period, width, and deflection angle can be further controlled by adjusting the beam spacing  $B$ . For in-phase propagation, centered on  $B = 2$ , the larger the value of  $|B|$ , the longer the period and the wider the width of the breathing soliton; for in-phase propagation, centered on  $B = 2$ , the larger the value of  $|B|$ , the larger the deflection angle of the breathing soliton. These findings not only deepen the understanding of nonlinear beam dynamics in photorefractive media but also open avenues for practical applications. By precisely tuning the refractive coefficient and chirp factor, our results suggest a novel strategy for multi-beam manipulation in optical communication systems. For instance, adjusting  $\beta$  could enable dynamic control of soliton binding strength and transmission stability, while modulating  $c$  may facilitate directional beam steering or signal routing. Such capabilities hold potential for optimizing high-speed data transmission, designing reconfigurable photonic devices, or developing advanced all-optical switching architectures. Future studies could explore experimental validations of these theoretical predictions and further integrate parameter-tuning mechanisms into practical optical setups. These findings provide a solid theoretical foundation for applying photorefractive media in the field of all-optical control and provide an important reference for studying the propagation dynamics of special light beams in complex media and the development of applications.

## REFERENCES

- [1] Pearcey T, "The structure of an electromagnetic field in the neighbourhood of a cusp of a caustic," *Phil. Mag. Sci.*, vol.37, no.268, pp 311-317, 1946.
- [2] Ring J D, Lindberg J, Mourka A, et al., "Auto-focusing and self-healing of Pearcey beams," *Opt. Express*, vol.20, no.17, pp 18955-18966, 2012.
- [3] Chen X Y, Deng D M, Zhuang J L, et al., "Focusing properties of circle Pearcey beams," *Opt. Lett.*, vol.43, no.15, pp 3626-3629, 2018.
- [4] Liu X, Zhao Q L, Monfared Y E, et al., "Flexible autofocusing properties of ring Pearcey beams by means of a cross phase," *Opt. Lett.*, vol.46, no.1, pp 70-73, 2021.
- [5] Wu Y, He S L, Wu J H, et al., "Autofocusing Pearcey-like vortex beam along a parabolic trajectory," *Chaos Solitons Fractals*, vol.145, pp 110781, 2021.
- [6] Jiang J J, Mo Z W, Xu D L, et al., "Elliptical Pearcey beam," *Opt. Commun.*, vol.504, pp 127475, 2022.
- [7] Liu Y J, Xu C J, Lin Z J, et al., "Auto-focusing and self-healing of symmetric odd-Pearcey Gauss beams," *Opt. Lett.*, vol.45, no.11, pp 2957-2960, 2020.
- [8] Chen X Y, Deng D M, Zhuang J L, et al., "Nonparaxial propagation of abruptly autofocusing circular Pearcey Gaussian beams," *Appl. Opt.*, vol.57, no.28, pp 8418-8423, 2018.
- [9] Zhou X Y, Pang Z H, Zhao D M, "Partially coherent Pearcey-Gauss beams," *Opt. Lett.*, vol.45, no.19, pp 5496-5499, 2020.
- [10] Sun C, Deng D M, Yang X B, et al., "Propagation dynamics of autofocusing circle Pearcey Gaussian vortex beams in a harmonic potential," *Opt. Express*, vol.28, no.1, pp 325-333, 2020.
- [11] Zang F, Liu L F, Deng F S, et al., "Dual-focusing behavior of a one-dimensional quadratically chirped Pearcey-Gaussian beam," *Opt. Express*, vol.29, no.16, pp 26048-26057, 2021.
- [12] Wen J J, Wang H W, Xiao Y, "Generation of Periodic Evolution Patterns By The Interaction of Pearcey-gaussian Beams Carrying Sidelobe in Parabolic Potential," *Phys. Scr.*, vol.98, pp 105510, 2023.
- [13] Li Y Q, Peng Y Q, Hong W Y, "Propagation of the Pearcey pulse with a linear chirp," *Results Phys.*, vol.16, pp 102932, 2020.
- [14] Zhang L P, Chen X Y, Deng D M, et al., "Dynamics of breathers-like circular Pearcey Gaussian waves in a Kerr medium," *Opt. Express*, vol.27, no.13, pp 17482-17492, 2019.
- [15] Xu C J, Wu J H, Wu Y, et al., "Propagation of the Pearcey Gaussian beams in a medium with a parabolic refractive index," *Opt. Commun.*, vol.464, pp 125478, 2020.
- [16] Huang Z C, He J J, Xu D L, et al., "Propagation of Pearcey Gaussian beams in a strongly nonlocal nonlinear medium," *Appl. Opt.*, vol.60, no.32, pp 10168-10175, 2021.
- [17] Huang Y M, Liu P W, Yi K W, et al., "Dynamics of Pearcey-Gaussian pulses in a multimode fiber," *Opt. Commun.*, vol.488, pp 126873, 2021.
- [18] Gao R, Ren S M, Guo T, et al., "Propagation dynamics of chirped Pearcey-Gaussian beam in fractional Schrödinger equation under Gaussian potential," *Optik*, vol.254, pp 168661, 2022.
- [19] Fattal Y, Rudnick A, Marom D, "Soliton shedding from Airy pulses in Kerr media," *Opt. Express*, vol.19, no.18, pp 17298-17307, 2011.
- [20] Jiang Q, Su Y, Ma Z, et al., "Propagation properties of Airy-Gaussian beams in centrosymmetric photorefractive media," *J. Mod. Optic.*, vol.65, no.19, pp 2243-2249, 2018.
- [21] Abdullah Z, Ripai A, Musyayyadah H A, et al., "Temporal behavior of diffusion-trapped Airy beams in photorefractive media," *Opt. Commun.*, vol.550, pp 129930, 2024.
- [22] Liu J L, Stace T, Dai J, et al., "Resonant Stimulated Photorefractive Scattering," *Phys. Rev. Lett.*, vol.127, pp 033902, 2021.
- [23] Jiang Q C, Su Y L, Ma Z W, et al., "Coherent interactions of multi-Airy-Gaussian beams in photorefractive media," *J. Opt.*, vol.49, pp 224-229, 2020.
- [24] Liu J Y, Liang K, "Interaction of Airy beams in photorefractive media," *Mod. Phys. Lett. B*, vol. 32, no.27, pp 1850323, 2018.
- [25] Grigoriev K S, Makarov V A, "Impact of various mechanisms of the photorefractive effect on polarization singularity generation during the self-focusing of a Gaussian beam in an isotropic medium," *J. Opt. Soc. Am. B*, vol.36, no.6, pp 1690-1694, 2019.